Using convex quadratic programming to model random media with Gaussian random fields

John A. Quintanilla*
Department of Mathematics, P.O. Box 311430, University of North Texas, Denton, Texas 76203, USA

W. Max Jones†
Texas Academy of Mathematics and Science, P.O. Box 305309, University of North Texas, Denton, Texas 76203, USA

(Received 24 July 2006; revised manuscript received 10 January 2007; published 30 April 2007)

Excursion sets of Gaussian random fields (GRFs) have been frequently used in the literature to model two-phase random media with measurable phase autocorrelation functions. The goal of successful modeling is finding the optimal field autocorrelation function that best approximates the prescribed phase autocorrelation function. In this paper, we present a technique which uses convex quadratic programming to find the best admissible field autocorrelation function under a prescribed discretization. Unlike previous methods, this technique efficiently optimizes over all admissible field autocorrelation functions, instead of optimizing only over a predetermined parametrized family. The results from using this technique indicate that the GRF model is significantly more versatile than observed in previous studies. An application to modeling a base-catalyzed tetraethoxysilane aerogel system given small-angle neutron scattering data is also presented

DOI: 10.1103/PhysRevE.75.046709 PACS number(s): 02.60.Pn, 05.40.−a, 81.05.Rm, 61.12.−q

I. INTRODUCTION

Models based on Gaussian random fields (GRFs) [1–7] have been employed in the literature to study a variety of two-phase material systems. These systems include foamed solids [8], mass and surface fractals [9], polymer blends [10], aerogels [12,13], sandstone [14], tungsten-silver composites [15], heather incidence [16], sulphide ores [17], and cellular solids [18].

Often the construction of a GRF model is based on an experimentally derived two-point phase probability function $S_2(x,y)$, defined to be the probability that two points $\mathbf{x},\mathbf{y}\in\mathbb{R}^d$ both lie in the solid phase. (We will assume throughout this paper that the material consists of a pore phase and a solid phase; however, the techniques described in this paper may be extended to other two-phase materials.) We will assume that S_2 is both translationally and rotationally independent, so that S_2 may be written as a function of $r=|\mathbf{x}-\mathbf{y}|$, the distance between the two points. For negative values of r, we extend S_2 to be an even function.

Clearly, $S_2(0)=\phi$ is the volume fraction of the solid phase. Also, for any random material without long-range order, we have

$$\lim_{r\to\infty} S_2(r) = \phi^2.$$

The phase autocorrelation function is defined as $\chi(r)=S_2(r)-\phi^2$. This function must be positive definite [19] so that its Fourier transform $\tilde{\chi}(k)$ is non-negative for all wave numbers k. Many techniques for measuring $\chi(r)$ for random materials have been proposed in the literature, including the use of small-angle scattering data described in Sec. V.

In this paper, we consider isotropic GRFs Y with mean 0 and variance 1. Such GRFs are completely characterized by the field autocorrelation function $G(r)=\langle Y(x)Y(y)\rangle$, where $r=|x-y|$. [This function should not be confused with the phase autocorrelation function $\chi(r)$.] A one-cut GRF model (also called an excursion set) is specified by the microstructure indicator function $I(x)=H[Y(x)-\alpha]$, where H is the Heaviside step function and α is a given threshold.

Some of the material systems listed above were modeled with a one-cut GRF model. Variants of this model were used for the other systems, including the two-cut model (defined in Sec. III C) and unions and intersections of individual GRF models.

We will denote by $\mathbf{P}$ the set of admissible field autocorrelation functions, or the set of all $G(r)$ so that there is a GRF with field autocorrelation function G. It can be shown that [20]

$$\mathbf{P}=\{G\in L^2[0,\infty): G(0)=1 \text{ and } G \text{ is positive definite}\}.$$

Therefore, to model a two-phase random material by a one-cut GRF model, the appropriate threshold level α and field autocorrelation function $G(r)$ must be determined. The value of α may be determined from the solid-phase volume fraction ϕ via

$$\phi = \frac{1}{\sqrt{2\pi}}\int_{-\infty}^{\alpha} e^{-t^2/2}dt. \tag{1}$$

In this paper, we will assume that ϕ is exactly measurable, so that the threshold α may be regarded as exact.

By contrast, determining the optimal field autocorrelation function $G(r)$ in $\mathbf{P}$ is more problematic. For the one-cut GRF model, the phase autocorrelation function is known to be equal to [21]

*Corresponding author. Electronic address: jquintanilla@unt.edu; URL: http://www.math.unt.edu/~johnq
†Permanent address: 555 Spring Park Center Blvd. #3105, Spring, TX 77373 USA. Electronic address: maximus93@yahoo.com

$$X(r) = \frac{1}{2\pi}\int_0^{G(r)} \frac{1}{\sqrt{1-t^2}} \exp\left(-\frac{\alpha^2}{1+t}\right)dt. \tag{2}$$

Loosely speaking, the primary goal of modeling is to choose $G(r)$ so that $X(r)$ is close to the desired $\chi(r)$. Unfortunately, this task is not as simple as setting $\chi(r)=X(r)$ in (2). Although the integral in (2) may be inverted since the integrand is monotone, thus permitting numerical evaluation of the upper limit of integration, the obtained function may not be in **P**. We will define $g(r)$ to be the function obtained from $\chi(r)$ via

$$\chi(r) = \frac{1}{2\pi}\int_0^{g(r)} \frac{1}{\sqrt{1-t^2}} \exp\left(-\frac{\alpha^2}{1+t}\right)dt. \tag{3}$$

We use lower-case g in (3) to indicate that this function may not be positive definite.

To get around this difficulty, previous researchers have found the function $G(r)$ which is optimal within a parametrized family in **P**. Examples of such families include, in one dimension [17],

$$G(r) = \exp(-ar^b),$$

$$G(r) = \begin{cases} 1 - \dfrac{3r}{2a} + \dfrac{r^3}{2a^3}, & 0 \leqslant r < a, \\ 0, & r \geqslant a, \end{cases}$$

where $a>0$ and $b>0$. In three dimensions, parametrized families include [9,12,14]

$$G(r) = \frac{3(\sin ar - \sin cr) - 3r(a\cos ar - c\cos cr)}{r^3(a^3 - c^3)},$$

$$G(r) = \frac{e^{-r/a} - (c/a)e^{-r/c}}{1-(c/a)}\frac{\sin(br)}{br},$$

$$G(r) = e^{-r/a}\left(1 + \frac{r}{a}\right)\frac{\sin(br)}{br},$$

where $a>c>0$ and $b>0$. Other examples of parametrized families within **P** may be found in Cressie [22], Roberts and Torquato [14], and Nott and Wilson [17].

Once a parametrized family has been chosen, some algorithm for estimating the optimal parameters is executed. Examples of such search algorithms include simulated annealing [13] and the expectation-maximization (EM) method [23]. The goal of these algorithms is usually to search for the parameters which minimize the L^2 norm

$$\int_0^\infty [\chi(r) - X(r)]^2 dr,$$

where $\chi(r)$ is the autocorrelation function to be fitted and $X(r)$ is computed for the one-cut GRF model by using (2). In practice, a discrete form of this integral is usually minimized.

There is a fundamental conceptual difficulty with using parametrized families: there is no reason *a priori* to think that the optimal $G(r)$ belongs to any predetermined family within **P**. In this paper, we introduce an algorithm for computing $G(r)$ that does not rely upon fitting parameters. This algorithm searches over discretizations of all functions in **P** to find the optimal field autocorrelation function. In practice, discretization does not introduce a significant loss of information since the modeler will usually measure $\chi(r)$ at a large but finite number of values. Using discretization reduces the present optimization problem to a convex quadratic program with linear constraints, a standard problem in operations research which may be solved by using either boundary or interior-point methods.

Algorithms appropriate for models in one and three dimensions are given in Secs. II C and IV A, respectively. Experience has shown that these algorithms are very efficient computationally. In other words, this technique simultaneously optimizes on a broad search of **P** (as opposed to a narrow search over a parametrized family within **P**) and typically finds the optimal solution within seconds of runtime on a desktop microcomputer.

In Sec. II, we describe the convex quadratic programming algorithm for one-dimensional models. Test results of the algorithm for various functions $\chi(r)$ for one-dimensional two-phase random media are presented in Sec. III. The generalization of the algorithm to three-dimensional systems and its application to two different models are presented in Sec. IV. We will see that the GRF model is more versatile than expected and can even produce a phase autocorrelation function $\chi(r)$ which exhibits the qualitative behavior of systems of impenetrable particles. Finally, in Sec. V, we compute an improved GRF model for a base-catalyzed tetraethoxysilane aerogel system, for which the function $\chi(r)$ is extracted from small-angle neutron scattering data.

II. ALGORITHM FOR ONE-DIMENSIONAL MODELS

A. Exact formulation in real space

We assume that the phase autocorrelation function $\chi(r)$ is known, either theoretically or from experimental measurement. As discussed in the Introduction, the function $g(r)$ may be obtained in principle from $\chi(r)$ by inverting the integral (3). However, the function thus obtained may violate the requirement of positive definiteness and thus may not belong to **P**.

Therefore, after numerically computing $g(r)$ from (3), the optimal function $G(r)$ in **P** may be defined as the solution of the following minimization problem:

$$\text{Minimize} \quad \int_0^\infty [g(r) - G(r)]^2 dr \tag{4}$$

$$\text{subject to} \quad \tilde{G}(k) \geqslant 0 \quad \text{for all } k \geqslant 0,$$

$$G(0) = 1.$$

Since G is an even function, the one-dimensional Fourier transform and its inverse transform are defined by

$$\tilde{G}(k) = \sqrt{\frac{2}{\pi}}\int_0^\infty G(r)\cos krdr, \tag{5}$$

$$G(r) = \sqrt{\frac{2}{\pi}} \int_0^\infty \tilde{G}(k) \cos krdk. \tag{6}$$

Since the set **P** is convex within $L^2[0,\infty)$, if g is any function in L^2, then there is a unique function G in **P** which minimizes the L^2 norm $\|g-G\|$ [24]. In other words, the minimization problem (4) has a unique solution.

B. Exact formulation in Fourier space

This minimization problem (4) may be written in Fourier space by using Parseval's equality

$$\int_0^\infty [f(r)]^2 dr = \int_0^\infty [\tilde{f}(k)]^2 dk$$

and the equation

$$G(0) = \sqrt{\frac{2}{\pi}} \int_0^\infty \tilde{G}(k) dk$$

obtained by setting $r=0$ into (6). The minimization problem thus takes the equivalent form

$$\text{Minimize} \int_0^\infty [\tilde{g}(k) - \tilde{G}(k)]^2 dk \tag{7}$$

$$\text{subject to } \tilde{G}(k) \geqslant 0 \quad \text{for all } k \geqslant 0,$$

$$\int_0^\infty \tilde{G}(k) dk = \sqrt{\frac{\pi}{2}}.$$

As before, this minimization problem has a unique solution. However, the analytical determination of the solution appears to be intractable.

C. Discrete formulation

As discussed in the Introduction, one way of getting around the difficulty of solving (7) analytically is by optimizing only over a parametrized subset of **P**. Conceptual and computational difficulties with this approach were also discussed in the Introduction.

Another way of solving (7) is by considering a discretized form of this minimization problem. Let $\tilde{g}_i = \tilde{g}(i\Delta k)$ $(i=0,\ldots,N)$ represent values of $\tilde{g}(k)$ on a evenly spaced partition of $[0, N\Delta k]$, where N is a large number and Δk is a prescribed step size. Using the trapezoid rule, (7) may be approximated by the following discrete minimization problem:

$$\text{Minimize} \sum_{i=0}^{N} (\tilde{g}_i - \tilde{G}_i)^2 \tag{8}$$

$$\text{subject to } \tilde{G}_i \geqslant 0 \quad \text{for } i = 0,\ldots,N,$$

$$\tilde{G}_0 + \tilde{G}_N + \sum_{i=1}^{N-1} 2\tilde{G}_i = \frac{\sqrt{2\pi}}{\Delta k}.$$

The minimization problem (8) is a convex quadratic program with linear constraints in the decision variables $\{\tilde{G}_i\}$, where $i=0,\ldots,N$. Therefore, there is a unique set of decision variables which minimizes this objective function [25].

This convex quadratic program may be solved by a variety of techniques. In this paper, we primarily used the software package LOQO [26], which utilizes an interior-point algorithm for solving quadratic programs. Experience has shown that the optimal $\{\tilde{G}_i\}$ is found within seconds on a 1-GHz desktop microcomputer; using discretizations of $N=5000$, 10 000, 20 000, and 40 000 for the modeling problems described in this paper, LOQO found the optimal solution in approximately 0.9, 2.4, 6.4, and 25.1 seconds, respectively. During the initial stages of testing, we also used MATHEMATICA to verify our results.

Once the optimal solution $\{\tilde{G}_i\}$ of (8) is found, discrete values for the autocorrelation function $\{G_i\}$ may be found by numerically computing the inverse Fourier integral (6). The phase autocorrelation function $X(r)$ for the resulting GRF model may be found by using (2) and interpolation.

Summarizing, given the solid volume fraction ϕ and the phase autocorrelation function $\chi(r)$, the convex quadratic programming algorithm is as follows:

(1) Choose parameters N and Δk to specify the discretization.

(2) Use (1) to compute α from ϕ.

(3) Use (3) to compute $g(r)$ from $\chi(r)$.

(4) Use the Fourier transform (5) to compute $\tilde{g}_i = \tilde{g}(i\Delta k)$ for $i=0,\ldots,N$.

(5) Solve the convex quadratic program (8) to find $\tilde{G}_i$ for $i=0,\ldots,N$.

(6) Use (6) to compute values of $G(r)$, the optimal field autocorrelation function.

(7) Use (2) to compute values of $X(r)$, the optimal phase autocorrelation function arising from a one-cut GRF model.

Naturally, numerical approximations of the integrals referenced above are typically used in lieu of analytical calculations.

The model may be validated by comparing the graph of $X(r)$ with the original phase autocorrelation function $\chi(r)$. Another technique for potentially validating the model involves comparing higher-order microstructural information, such as the chord-length density function [14], for the GRF model with the original model. This analysis will be the subject of a future paper.

III. TEST RESULTS IN ONE DIMENSION

In this section, we present the results of using the algorithm in Sec. II C to fit various one-dimensional test models to the one-cut GRF model.

A. Boolean model of equal-sized rods

We begin with a Boolean model ([27], Chap. 3) of unit-length rods with Poisson intensity ρ. For this model, the

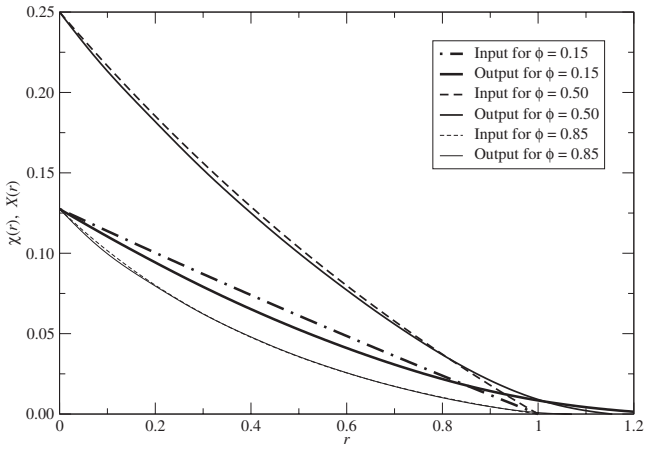

FIG. 1. The phase autocorrelation functions $\chi(r)$ for a Boolean model of unit-length rods (dashed lines) at ϕ=0.15, ϕ=0.50, and ϕ=0.85, and the best-fit autocorrelation functions $X(r)$ for a one-cut GRF model. The GRF model becomes a better approximation to the Boolean model as the volume fraction of the rod phase increases.

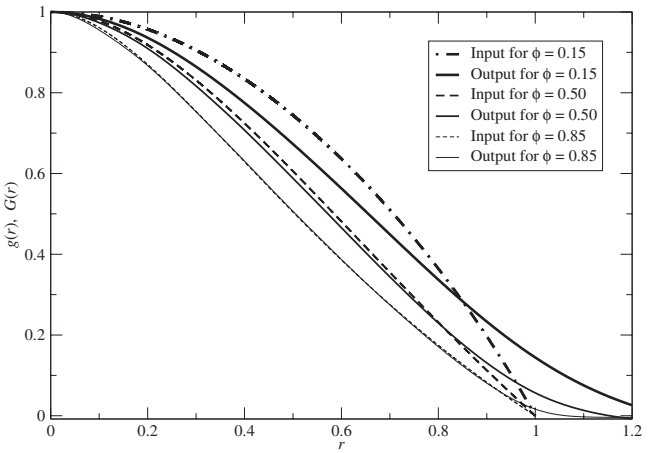

FIG. 2. As in Fig. 1, except showing the field autocorrelation function. The dashed curves of $g(r)$ correspond to the exact $\chi(r)$ but are not positive definite. The solid curves $G(r)$ represent the closest positive definite functions to the dashed curves.

volume fraction of the solid phase is $\phi=1-e^{-\rho}$, while the phase autocorrelation function is

$$\chi(r) = \begin{cases} e^{-\rho(1+r)} - e^{-2\rho}, & 0 \leqslant r \leqslant 1, \\ 0, & r > 1. \end{cases}$$

In Fig. 1, we present these inputs $\chi(r)$ (in dashed lines) with the outputs $X(r)$ for the optimal GRF model. We choose three volume fractions: ϕ=0.15, ϕ=0.50, and ϕ=0.85. We see that the GRF model fits the Boolean model better at large values of ϕ. This makes intuitive sense; at small values of ϕ, the Boolean model will consist of rarely overlapping lines of equal size, a geometry not especially suited for the GRF model. On the other hand, at large values of ϕ, there will be considerable overlap in the Boolean model, and the clusters that are formed will have a range of sizes. For these Boolean models, the GRF model can be more accurately fitted.

In Fig. 2, we show the corresponding graphs for $g(r)$ and $G(r)$; these are represented with dashed and solid lines, respectively. As discussed above, the functions $g(r)$ exactly correspond to $\chi(r)$ but may not be positive definite. The discretized functions $G(r)$ represent the closest positive definite functions (under the L^2 norm) to the input functions $g(r)$.

In Fig. 3, we show the corresponding graphs of $\tilde{g}(k)$ and $\tilde{G}(k)$ for ϕ=0.15. The graphs represent the input and output of the convex quadratic programming algorithm. In particular, the output function is the closest (under the discretization) non-negative function $\tilde{G}(k)$ whose integral over the entire wave-number domain matches the integral for the input function. As described in Sec. II C, the functions $G(r)$ in Fig. 2 and $X(r)$ in Fig. 1 are computed using this optimized function.

For ϕ=0.50 and ϕ=0.85, the functions $\tilde{g}(k)$ assumes negative values for fewer inputs k. Correspondingly, the graphs of $\tilde{g}(k)$ and $\tilde{G}(k)$ for the other volume fractions are qualitatively similar to Fig. 3, but the input and output functions are not as markedly different from each other.

B. Impenetrable rods

Next, we test the ability of GRFs to model a system of impenetrable unit-length rods at thermal equilibrium. If the volume fraction of the rod phase is ϕ, then the phase autocorrelation function is [28]

$$\chi(r) = -\phi^2 + (1-\phi)\sum_{j=0}^{M} \frac{1}{j!}\left[\frac{(r-j)\phi}{1-\phi}\right]^k \exp\left[-\frac{(r-j)\phi}{1-\phi}\right],$$

where $M \leqslant r < M+1$.

Notice that there is a cusp in the graph of $\chi(r)$ at r=1. Since this model consists of nonoverlapping rods, we would expect that the GRF model is not particularly well-suited to

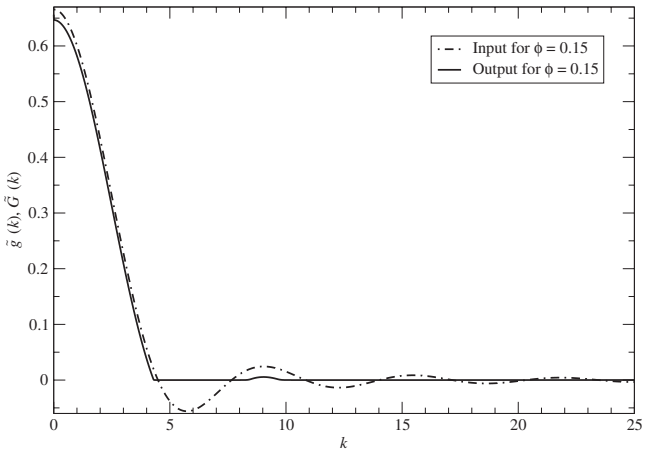

FIG. 3. As in Fig. 1, except showing the Fourier transform of the field autocorrelation function for ϕ=0.15. The dashed curve $\tilde{g}(k)$ corresponds to the exact $\chi(r)$ but can be negative at some wave numbers k. Discretizations of these curves are used as input in the convex quadratic programming algorithm. The output $\tilde{G}(k)$ of the algorithm, which solves the convex quadratic program (8), is shown with the solid curve. (The corresponding graphs for ϕ=0.50 and ϕ=0.85 are similar, but the input and output graphs are not as markedly different at these higher volume fractions.)

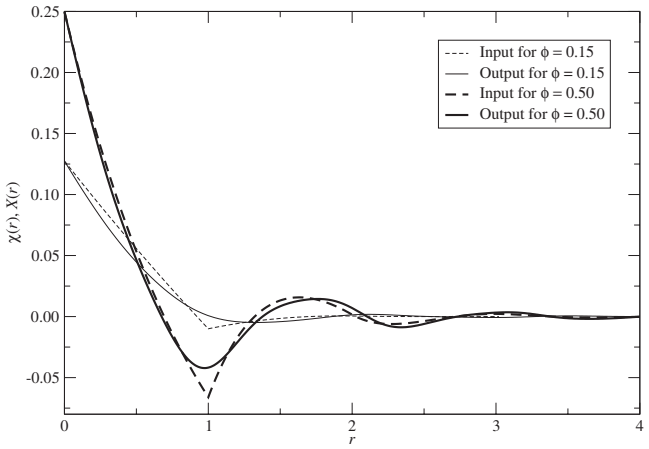

FIG. 4. The phase autocorrelation functions $\chi(r)$ for totally impenetrable unit-length rods in thermal equilibrium (dashed lines) at $\phi=0.15$ and $\phi=0.50$, and the best-fit autocorrelation functions $X(r)$ for a one-cut GRF model (solid lines). The fits are not as tight as in Fig. 1; this is not surprising since the GRF model is ill-suited for impenetrable rods.

this model. This may be seen in Fig. 4, where we plot $\chi(r)$ and $X(r)$ for $\phi=0.15$ and $\phi=0.50$. Nevertheless, we see that the graph of $X(r)$ for $\phi=0.50$ exhibits the oscillatory behavior indicative of systems of impenetrable particles. In fact, as seen in Fig. 5, the graphs of $\chi(r)$ and $X(r)$ are remarkably similar for $\phi=0.85$.

C. Two-cut GRF model

Our last one-dimensional example will be matching a one-cut GRF model to a two-cut GRF model. If $Y(x)$ is the underlying Gaussian random field, the two-cut model is defined by assigning phases according to whether the condition $\alpha<Y(x)<\beta$ is satisfied, where α and β are given cut parameters. For the two-cut model, the phase autocorrelation function is [11]

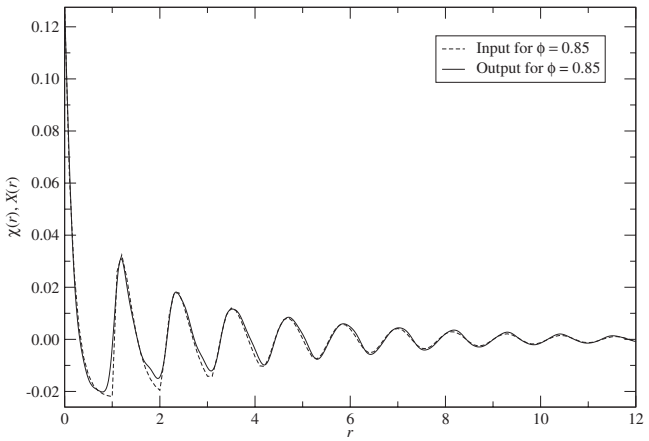

FIG. 5. As in Fig. 4, except for $\phi=0.85$. The fit is fairly tight, showing that the GRF model is versatile enough to exhibit the qualitative behavior of certain systems of impenetrable particles.

$$\chi(r)=\frac{1}{2\pi}\int_0^{f(r)}\frac{1}{\sqrt{1-t^2}}\left[\exp\left(-\frac{\alpha^2}{1+t}\right)-2\exp\left(-\frac{\alpha^2-2\alpha\beta t+\beta^2}{2(1-t^2)}\right)+\exp\left(-\frac{\beta^2}{1+t}\right)\right]dt. \tag{9}$$

The volume fraction of the model is given by

$$\phi=\frac{1}{\sqrt{2\pi}}\int_\alpha^\beta e^{-t^2/2}dt.$$

Also, the function $f(r)$ is positive definite and represents the field autocorrelation function of $Y(x)$.

To test the algorithm, we used $f(r)=e^{-r^2}$ and tried three different sets of parameters for a and b, $(a,b)=(0,1)$, $(a,b)=(-1,1)$, and $(a,b)=(-1,2)$. In these examples, the function $\tilde{g}(k)$ was only negative for very few wave numbers k. Therefore, a one-cut GRF model can closely match the phase autocorrelation functions for these two-cut models. Through this computation, we also directly confirm that the two-cut GRF model can produce images not exactly obtainable with a one-cut model.

We also tried the function $f(r)=e^{-r}$ in the definition (9). For all values of a and b attempted, the function $\tilde{g}(k)$ turned out to be positive, so that $g(r)$ was already positive definite. Since Gaussian random fields are statistically specified by their field-field correlation functions, this means that the geometries described by these two-cut models with this choice of $f(r)$ are exactly obtainable by a one-cut model.

IV. APPLICATION TO THREE-DIMENSIONAL MODELS

A. Details of algorithm

The extension of the above work to a three-dimensional GRF model is straightforward. Under the assumption of isotropy, the required Fourier transforms are

$$\tilde{G}(k)=\sqrt{\frac{2}{\pi}}\int_0^\infty r^2G(r)\frac{\sin kr}{kr}dr, \tag{10}$$

$$G(r)=\sqrt{\frac{2}{\pi}}\int_0^\infty k^2\tilde{G}(k)\frac{\sin kr}{kr}dk. \tag{11}$$

Therefore, the constraint $G(0)=1$ has the discrete form

$$N^2\tilde{G}_N+\sum_{i=1}^{N-1}2i^2\tilde{G}_i=\frac{\sqrt{2\pi}}{(\Delta k)^3},$$

where N and Δk are as before.

In three dimensions, we will seek the isotropic function $G(x)$ which minimizes the space integral

$$\int_{\mathbb{R}^3}[g(\mathbf{x})-G(\mathbf{x})]^2d\mathbf{x}=4\pi\int_0^\infty r^2[g(r)-G(r)]^2dr.$$

Using Parseval's equality, this is equivalent to minimizing

$$\int_0^\infty k^2[\tilde{g}(k) - \tilde{G}(k)]^2 dk.$$

Taking the discrete form of this integral, the minimization problem for fitting a one-cut GRF in three dimensions is therefore

$$\text{Minimize} \sum_{i=1}^{N} i^2(\tilde{g}_i - \tilde{G}_i)^2 \tag{12}$$

$$\text{subject to } \tilde{G}_i \geqslant 0 \quad \text{for } i = 1,\ldots,N,$$

$$N^2\tilde{G}_N + \sum_{i=1}^{N-1} 2i^2\tilde{G}_i = \frac{\sqrt{2\pi}}{(\Delta k)^3}.$$

The convex quadratic programming algorithm in three dimensions is as follows:

(1) Choose parameters N and Δk to specify the discretization.

(2) Use (1) to compute α from ϕ.

(3) Use (3) to compute $g(r)$ from $\chi(r)$.

(4) Use the Fourier transform (10) to compute $\tilde{g}_i = \tilde{g}(i\Delta k)$ for $i = 1, \ldots, N$.

(5) Solve the convex quadratic program (12) to find $\tilde{G}_i$ for $i = 1, \ldots, N$.

(6) Use (11) to compute values of $G(r)$, the optimal field autocorrelation function.

(7) Use (2) to compute values of $X(r)$, the optimal phase autocorrelation function arising from a one-cut GRF model. The model may be validated by comparing the graph of $X(r)$ with the original phase autocorrelation function $\chi(r)$.

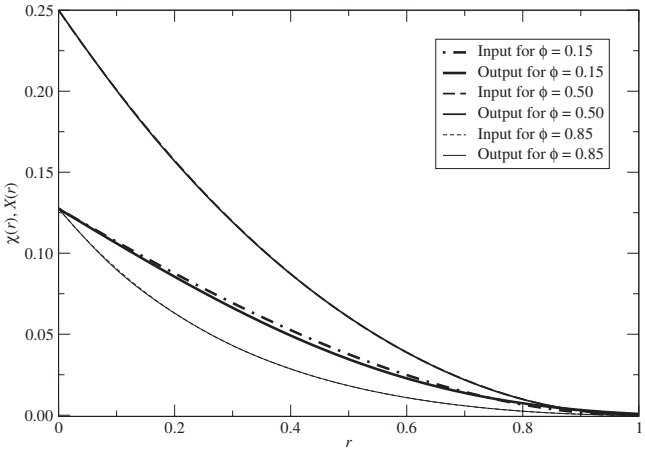

FIG. 6. The phase autocorrelation functions $\chi(r)$ for a Boolean model of unit-diameter spheres (dashed lines) at $\phi=0.15$, $\phi=0.50$, and $\phi=0.85$, and the best-fit autocorrelation functions $X(r)$ for a one-cut GRF model. The fits are much tighter than the analogous one-dimensional models; on the scale of this figure, the fits $X(r)$ are not easily distinguishable from the original $\chi(r)$ for $\phi=0.50$ and $\phi=0.85$.

B. Fully penetrable spheres

We now discuss the application of this algorithm to two different systems based on spheres of unit diameter. Our first three-dimensional test model is the Boolean model. If the underlying Poisson process has intensity ρ, the volume fraction of the solid phase is $\phi = 1 - \exp(-\pi\rho/6)$, while the phase autocorrelation function is ([19], Sec. 5.1.1)

$$\chi(r) = \begin{cases} \exp\left(-\dfrac{\pi\rho(2+3r-r^3)}{12}\right) - \exp\left(-\dfrac{\pi\rho}{3}\right), & 0 \leqslant r \leqslant 1, \\ 0, & r > 1. \end{cases}$$

This input function $\chi(r)$ and the output autocorrelation function $X(r)$ from the GRF model are shown in Fig. 6 for $\phi=0.15$, $\phi=0.50$, and $\phi=0.85$. As before, the quality of the fit improves as ϕ increases. These fits are much tighter than the analogous models in one dimension (shown in Fig. 1). In fact, on the scale of this figure, the functions $\chi(r)$ and $X(r)$ are barely distinguishable for $\phi=0.50$ and $\phi=0.85$.

C. Impenetrable spheres

The second test model we consider is a certain "well-stirred" model of impenetrable spheres of unit diameter. If $\phi \leqslant 0.125$, the phase autocorrelation function is [29,30]

$$\chi(r) = \begin{cases} \phi(1-\phi) - \dfrac{3\phi r}{2} + \dfrac{\phi(1+3\phi)r^3}{2} - \dfrac{9\phi^2 r^4}{10} + \dfrac{\phi^2 r^6}{35}, & 0 \leqslant r \leqslant 1, \\ \dfrac{\phi^2(r-2)^4(9-17r-16r^2-2r^3)}{70r}, & 1 \leqslant r \leqslant 2, \\ 0, & r \geqslant 2. \end{cases}$$

However, if $\phi > 0.125$, then this model is not realizable, a fact which has been confirmed by simulations [31].

This input function $\chi(r)$ and the output autocorrelation function $X(r)$ from the GRF model are shown in Fig. 7 for $\phi=0.05$ and $\phi=0.125$. Not surprisingly, since the GRF model is not particularly suited for impenetrable sphere models, the fits are not as close as in the Boolean model. However, it is again surprising that a GRF model can be found whose phase autocorrelation function exhibits the qualitative behavior expected of systems of impenetrable particles.

Though we do not do so here, this algorithm may be applied to other models of impenetrable spheres besides the "well-stirred" model. Expressions of $\chi(r)$ for other commonly used models are presented by Markov and Willis [30] and by Torquato ([19], Sec. 5.2.1).

V. APPLICATION TO AEROGELS

In Secs. III and IV, we considered the application of the GRF model to various theoretical models of random materials. In this section, we model a specific tetraethoxysilane (TEOS) aerogel using small-angle neutron scattering (SANS) experimental data. We will see that the resulting GRF model has an experimental scattering function that closely resembles the experimental data. Therefore, using scattering data as input, the resulting GRF model may be used to generate predictive realizations of this aerogel.

A. Recovery of $\chi(r)$ from scattering data

In the absence of multiple scattering (a reasonable assumption for aerogels and other materials with a low volume fraction), the scattering intensity is given by [32]

$$I(q) = I_0 + V\eta^2 \int_0^\infty 4\pi r^2 \chi(r) \frac{\sin qr}{qr} dr, \tag{13}$$

where I_0 is background noise, V is the volume of the material, and η is the scattering density of the solid phase. In principle, given the intensity function, the phase autocorrelation function may be computed using the inverse Fourier transformation,

$$\chi(r) = \frac{1}{2\pi^2 V\eta^2} \int_0^\infty [I(q) - I_0] q^2 \frac{\sin qr}{qr} dq. \tag{14}$$

However, in practice, this is problematic since $\chi(r)$ must be positive definite, a requirement that may be violated after the numerical computations.

We now assume that discrete scattering intensity data $\{q_j, I(q_j)\}$ is experimentally measured. To use the convex quadratic programming to match this scattering data, an extra layer of computation is added to the algorithm, namely, the extraction of $\chi(r)$ from $I(q)$ using (14). This extraction entails measurement of the background noise I_0 and also the constant $V\eta^2$. To estimate the background noise, we will use the asymptotic behavior ([19], Sec. 2.2.5)

$$I(q) - I_0 \sim \frac{a}{q^4} + \frac{b}{q^6} + \frac{c}{q^8} \quad \text{as } q \to \infty. \tag{15}$$

The background noise I_0 is thus estimated to be the number that gives the best approximation to this asymptotic behavior. Furthermore, the values of a, b, and c are obtained by least-squares fitting to some subset of the largest frequencies q_j used in the experiment.

In summary, given experimental data on a limited set of frequencies within $[0, Q]$, the integral (14) may be approximated by

$$\chi(r) \approx \frac{1}{2\pi^2 V\eta^2} \left[\int_0^Q [I(q) - I_0] q^2 \frac{\sin qr}{qr} dq + \int_Q^\infty \left(\frac{a}{q^2} + \frac{b}{q^4} + \frac{c}{q^6} \right) \frac{\sin qr}{qr} dq \right], \tag{16}$$

where $Q = \max\{q_j\}$. For discrete experimental data, the first integral may be approximated by the trapezoidal rule for uneven step sizes. We note that, for bounded intensity data, omission of the second integral would necessarily cause $\chi'(0)=0$, a mathematical impossibility ([27], Sec. 6.2). Therefore, determining the approximate asymptotic behavior of the scattering data is an essential step in determining $\chi(r)$.

To compute $V\eta^2$, we will use the fact that $\chi(0) = \phi - \phi^2$, where again ϕ is the (directly measurable) volume fraction of the solid phase of the aerogel. Substituting into (16), we find that

$$\phi - \phi^2 = \frac{1}{2\pi^2 V\eta^2} \left[\int_0^Q q^2 [I(q) - I_0] dq + \int_Q^\infty \left(\frac{a}{q^2} + \frac{b}{q^4} + \frac{c}{q^6} \right) dq \right].$$

This equation permits the evaluation of the constant $V\eta^2$.

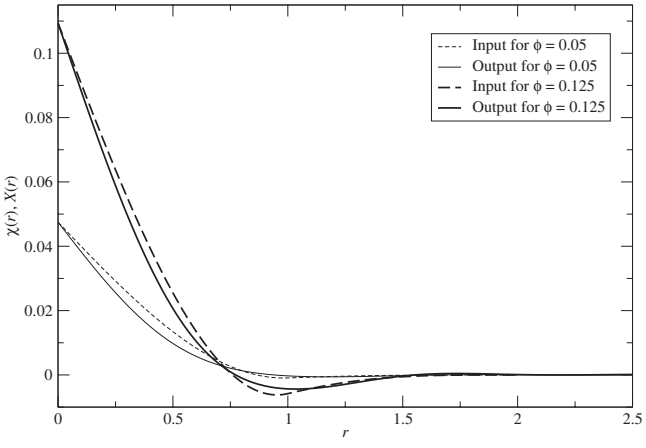

FIG. 7. The phase autocorrelation functions $\chi(r)$ for the well-stirred model of totally impenetrable spheres of unit diameter (dashed lines) at $\phi=0.05$ and $\phi=0.125$, and the best-fit autocorrelation functions $X(r)$ for a one-cut GRF model (solid lines). The fits are not as tight as in Fig. 6; this is not surprising since the GRF model is ill-suited for impenetrable spheres.

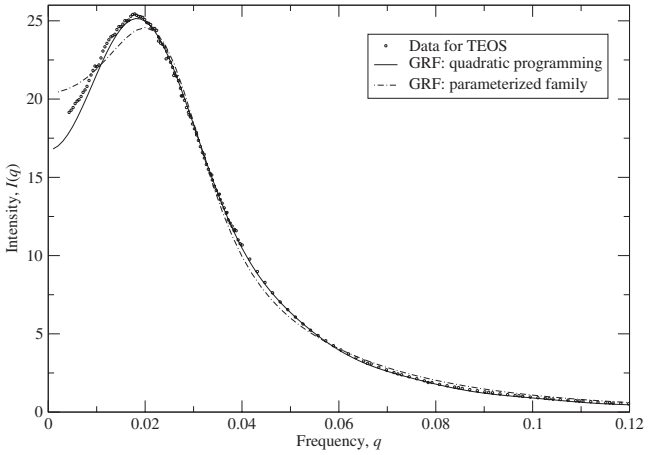

FIG. 8. Small-angle neutron scattering data for a TEOS aerogel, and the theoretical scattering function for the optimal GRF model (solid line). Also shown as a dashed line is the scattering function for a previously obtained GRF model found by optimizing over a certain parametrized family of admissible field autocorrelation functions. We see that the convex quadratic programming algorithm provides a significantly tighter fit than modeling over a specific parametrized family.

This function $\chi(r)$ thus obtained from experimental intensity data may or may not be positive definite due to both experimental errors and the computational inaccuracies inherent to the approximations used above. Nevertheless, we may proceed with the algorithm in Sec. IV A to obtain the closest-fitting $X(r)$ arising from a one-cut GRF model.

B. Results for TEOS

In Fig. 8, we show SANS data for the TEOS aerogel (in dots) and the theoretical scattering curve $I(q)$ for the optimal GRF model. This scattering curve was obtained by computing $X(r)$, as described in Sec. IV A, and then numerically evaluating (13), with $X(r)$ in place of $\chi(r)$. We see that this optimal GRF model provides an excellent fit to the experimental data. The fit is acceptable even for low frequencies q, a region known to be difficult for modeling.

For comparison, the theoretical scattering curve of a previously obtained GRF model for the TEOS aerogel is also presented [13]. In this previously obtained model, the field autocorrelation function was found by optimizing over the three-parameter family of three-dimensional field autocorrelation functions given in Sec. I. (Also, this model was obtained from the intersection of two GRF models which use two cuts, as in Sec. III C.)

We see in Fig. 8 that this previous theoretical scattering curve generally tracked the experimental data but was measurably different in several places, especially for $q<0.02$ and for $0.04<q<0.05$. By contrast, the algorithm in Sec. IV A produces a much tighter fit to the experimental data obtained.

The GRF model may be used to produce predictive visualizations of the TEOS aerogel, a fundamental goal of analyzing the microstructure of materials. Our visualization, shown in Fig. 9, was generated by using the turning-bands method [33,34] and has a strong morphological resemblance to a transmission electron microscopy image of the aerogel [13].

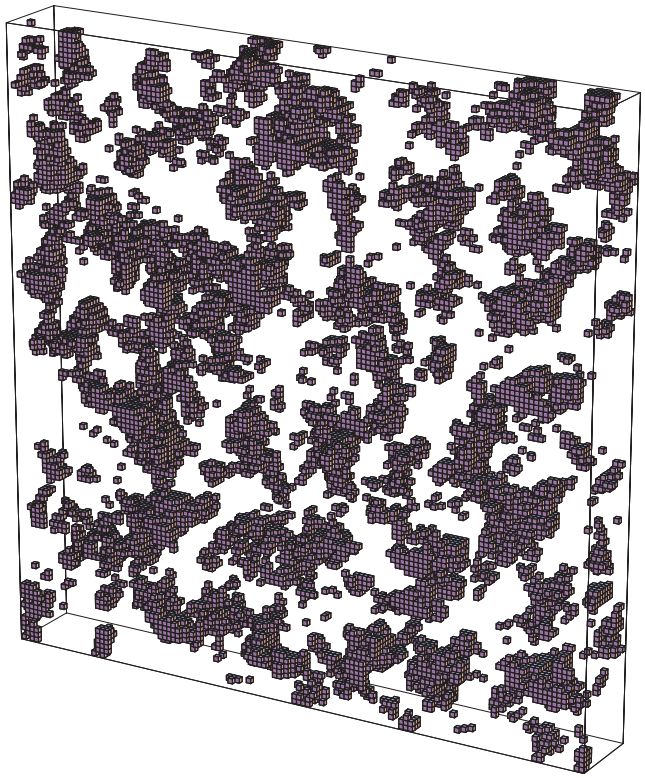

FIG. 9. (Color online) A realization of the GRF model for the TEOS aerogel, generated by using the turning-bands method. The dimensions of this realization are $1500\times1500\times187.5$ Å. This realization bears a strong morphological resemblance to transmission electron microscopy images of the actual aerogel [13].

The improved GRF model found in this paper can also be expected to predict other properties of the aerogel besides the scattering function, such as connectivity and pore-size information. These and other microstructure characterizations will be considered in future papers.

VI. CONCLUSIONS AND FUTURE STUDIES

We have used convex quadratic programming to efficiently find the optimal Gaussian random field to fit a prescribed phase autocorrelation function $\chi(r)$. The techniques used in this paper have the simultaneous advantages of computational efficiency and searching through all possible field autocorrelation functions. Tests of this algorithm in one and three dimensions show that the GRF model is surprisingly versatile, fitting even systems of impenetrable particles with reasonable accuracy. We have illustrated the power of this algorithm by generating a GRF model whose theoretical scattering curve closely matches experimentally obtained scattering data.

This versatility had not been observed in previous studies of the GRF model, in which searches were restricted to within a predetermined parameterized family of admissible field autocorrelation functions. Therefore, it seems reason-

able that such families should be used only when there are physical or other considerations that restrict the underlying field autocorrelation function.

The optimal Gaussian random field may be found without undue complication if the autocorrelation function $\chi(r)$ is exactly known. However, if $\chi(r)$ is implicitly defined through scattering data, then the parameters I_0, a, b, and c in (15) must first be obtained before applying the algorithm. In a future paper, we will explore modeling issues that arise from making such estimates.

In this paper, only the phase autocorrelation function $\chi(r)$ [or, equivalently, the intensity function $I(q)$] was used to find the optimal GRF model. However, it is well known that $\chi(r)$ alone does not uniquely specify higher-order microstructural information like clustering and percolation. For example, the phase autocorrelation function $\chi(r)=ae^{-cr}$ may be obtained from the Poisson line tesselation model [27] as well as a Debye model [35] constructed via stochastic optimization, another technique for finding random media with a prescribed $\chi(r)$ [35–38]. In future work, we will consider the application of the convex quadratic programming approach to find optimal GRF models by using higher-order microstructural information. [For completeness, we note that it has been mathematically proven that $\chi(r)$ completely determines microstructures within several types of models, such as GRF models [22] and models of convex polygons [39]. Furthermore, recent computational work using stochastic optimization [38] suggests that periodic microstructures may be uniquely specified by $\chi(r)$.]

The convex quadratic programming algorithm described in this paper may be used in conjunction with stochastic optimization. Previous implementations of stochastic optimization have used a random array of pixels as an initial configuration. Using the techniques described in this paper, a realization of an appropriate GRF model can instead be chosen as the initial configuration. By choosing a configuration whose phase autocorrelation function $X(r)$ reasonably approximates the target $\chi(r)$, valuable computational time and effort may be saved when using stochastic optimization. This application of this algorithm and others will be discussed in future papers.

ACKNOWLEDGMENTS

The authors are grateful to Neal Brand, Jay Liu, Robert Kallman, John Neuberger, Rick Reidy, and Salvatore Torquato for many helpful discussions. The authors also thank Robert Vanderbei for assistance with his LOQO software package.

[1] J. W. Cahn, J. Chem. Phys. **42**, 93 (1965).
[2] J. A. Quiblier, J. Colloid Interface Sci. **98**, 84 (1984).
[3] N. F. Berk, Phys. Rev. Lett. **58**, 2718 (1987).
[4] N. F. Berk, Phys. Rev. A **44**, 5069 (1991).
[5] M. Teubner, Europhys. Lett. **14**, 403 (1991).
[6] M. B. Isichenko, Rev. Mod. Phys. **64**, 961 (1992).
[7] R. Blumenfeld and S. Torquato, Phys. Rev. E **48**, 4492 (1993).
[8] A. P. Roberts and M. A. Knackstedt, J. Mater. Sci. Lett. **14**, 1357 (1995).
[9] A. P. Roberts and M. A. Knackstedt, Physica A **233**, 848 (1996).
[10] M. A. Knackstedt and A. P. Roberts, Macromolecules **29**, 1369 (1996).
[11] A. P. Roberts and M. A. Knackstedt, Phys. Rev. E **54**, 2313 (1996).
[12] A. P. Roberts, Phys. Rev. E **55**, R1286 (1997).
[13] J. Quintanilla, R. F. Reidy, B. P. Gorman, and D. W. Mueller, J. Appl. Phys. **93**, 4584 (2003).
[14] A. P. Roberts and S. Torquato, Phys. Rev. E **59**, 4953 (1999).
[15] A. P. Roberts and E. J. Garboczi, J. Mech. Phys. Solids **47**, 2029 (1999).
[16] D. J. Nott and T. Rydén, Biometrika **86**, 661 (1999).
[17] D. J. Nott and R. J. Wilson, Signal Process. **80**, 125 (2000).
[18] A. P. Roberts and E. J. Garboczi, Acta Mater. **49**, 189 (2001).
[19] S. Torquato, *Random Heterogeneous Materials: Microstructure and Macroscopic Properties* (Addison-Wesley, New York, 2002).
[20] B. D. Ripley, *Spatial Statistics* (Wiley, New York, 1981), Chap. 2.
[21] H. Cramér and M. R. Leadbetter, *Stationary and Related Stochastic Processes* (Wiley, New York, 1967), p. 27.
[22] N. A. C. Cressie, *Statistics for Spatial Data* (Wiley, New York, 1993), Sec. 2.5.1.
[23] D. J. Nott and R. J. Wilson, Signal Process. **63**, 199 (1997).
[24] E. Kreyszig, *Introductory Functional Analysis with Applications* (Wiley, New York, 1978), Sec. III C.
[25] F. S. Hillier and G. J. Lieberman, *Introduction to Operations Research*, 8th ed. (McGraw-Hill, New York, 2004), Sec. 12.2.
[26] R. J. Vanderbei, Optim. Methods Software **12**, 451 (1999).
[27] D. Stoyan, W. S. Kendall, and J. Mecke, *Stochastic Geometry and Its Applications* (Wiley, New York, 1995).
[28] J. Quintanilla and S. Torquato, Phys. Rev. E **53**, 4368 (1996).
[29] S. Torquato and G. Stell, J. Chem. Phys. **82**, 980 (1985).
[30] K. Z. Markov and J. R. Willis, Math. Models Meth. Appl. Sci. **8**, 359 (1998).
[31] J. Crawford, S. Torquato, and F. H. Stillinger, J. Chem. Phys. **119**, 7065 (2003).
[32] A. Guinier, G. Fournet, C. B. Walker, and K. L. Yudowitch, *Small-Angle Scattering of X-Rays* (Wiley, New York, 1955), Sec. 2.1.2.
[33] A. Mantoglou and J. L. Wilson, Water Resour. Res. **18**, 1379 (1982)
[34] A. F. B. Tompson, R. Ababou, and L. W. Gelhar, Water Resour. Res. **25**, 2227 (1989).
[35] C. L. Y. Yeong and S. Torquato, Phys. Rev. E **57**, 495 (1998).
[36] D. Cule and S. Torquato, J. Appl. Phys. **86**, 3428 (1999).
[37] M. G. Rozman and M. Utz, Phys. Rev. E **63**, 066701 (2001).
[38] M. G. Rozman and M. Utz, Phys. Rev. Lett. **89**, 135501 (2002).
[39] W. Nagel, J. Appl. Probab. **30**, 730 (1993).